Optimized Feature Extraction via Custom Low-Cost sEMG Hardware for Real-Time Myoelectric Interfaces

Thi-Mai-Phuong Dao
School of Electrical and Electronic Engineering (SEEE), Hanoi University of Industry, Hanoi, Vietnam
daophuong@haui.edu.vn

Van-Kien Nguyen
Technology Section, Duy Hoang High Technology Consultancy Joint Stock Company, Hanoi, Vietnam
nguyenvankien197197@gmail.com

Ngoc-Khoat Nguyen
Faculty of Control and Automation, Electric Power University, Hanoi, Vietnam
khoatnn@epu.edu.vn (corresponding author)

Le Loc
Faculty of Postgraduate Studies, Lac Hong University, Dongnai, Vietnam
codiendientu@lhu.edu.vn

Tien-Dung Nguyen
Faculty of Control and Automation, Electric Power University, Hanoi, Vietnam
dungnt@epu.edu.vn

Tri Nguyen
Control Automation in Production and Improvement of Technology Institute (CAPITI), Academy of Military Science and Technology, Hanoi, Vietnam
tripb28@gmail.com

Thi-Duyen Bui
Faculty of Control and Automation, Electric Power University, Hanoi, Vietnam
duyenbt@epu.edu.vn

Duy-Trung Nguyen
Faculty of Control and Automation, Electric Power University, Hanoi, Vietnam
trungnd@epu.edu.vn

Huu-Thang Nguyen
Faculty of Electrical Engineering, Electronics and Refrigeration, Thanh Hoa College of Industry, Thanh Hoa, Vietnam
thangnh.25TS0000011@epu.edu.vn

Received: 13 November 2025 | Revised: 4 December 2025 and 17 December 2025 | Accepted: 24 December 2025

 DOI: https://doi.org/10.48084/etasr.16242

ABSTRACT

Surface Electromyography (sEMG) is a widely used modality to infer human motor intent in Human–Machine Interaction (HMI) systems. This study presents a cost-effective, custom-fabricated sEMG acquisition module with three differential channels strategically positioned to capture bioelectric activity from key forearm muscles. The analog front-end is designed with a high-gain amplification stage (2200×) and a bandpass filter spanning 48 to 482 Hz to suppress motion artifacts and ambient noise while preserving relevant myoelectric information. Acquired signals are processed through a lightweight digital pipeline including bandpass and 50 Hz notch filtering, followed by segmentation using a 200 ms sliding window with 50% overlap to balance temporal resolution and computational efficiency. Feature extraction focuses on commonly used time-domain descriptors (MAV, WL, RMS, VAR, and IEMG) and frequency-domain features (MNF and MDF). Experimental evaluation shows that the proposed system achieves a Signal-to-Noise Ratio (SNR) of 17.8–22.5 dB across three channels, while amplitude-based time-domain features (RMS and WL) exhibit less than 5% variability across repeated trials. These results indicate that the proposed hardware–software framework provides stable and reliable feature extraction suitable for real-time embedded applications. The system is therefore well-suited for wearable HMI scenarios such as myoelectric prostheses, robotic exoskeletons, and assistive robotic devices requiring low latency and low computational complexity.

Keywords-sEMG; custom-fabricated sEMG sensor; biomedical signal processing; feature extraction

I. INTRODUCTION

In the era of Industry 4.0 and the rapid development of robotics, assistive devices, and Human-Machine Interfaces (HMIs), the connection between human motor intent and machine systems has become increasingly important. HMI not only involves transmitting information from humans to machines, but also requires accurately interpreting and translating users' motor intentions into control commands for machines or assistive devices.

Among the various interaction modalities that are both intuitive and biologically relevant, surface Electromyography (sEMG) has been demonstrated to be a highly promising channel for decoding human motor intent. sEMG is a bioelectric signal recorded from the skin surface when motor units in muscles are activated. Each motor unit consists of a motor neuron and the muscle fibers it innervates; when the neuron fires, the corresponding fibers generate action potentials that propagate along the muscle bundle. The superposition of hundreds to thousands of these action potentials forms the measurable sEMG signal captured by electrodes on the skin [1, 2]. Unlike intramuscular EMG (iEMG), which uses needle electrodes to record signals directly within muscles, sEMG is non-invasive, easier to implement, and safer for clinical or HMI applications. sEMG signals typically precede muscle contraction by approximately 50–100 ms [3-4], providing information on co-contraction levels of antagonistic muscle groups—data not available through kinematic or kinetic measurements [5]. Thus, sEMG can be used to predict human movement and subsequently control robotic systems based on these predictions.

sEMG-based technologies have been widely applied across multiple fields. In rehabilitation, sEMG is used for biofeedback, neuromuscular disorder diagnosis, and monitoring recovery progress, particularly in conditions such as stroke, spinal cord injury, and musculoskeletal disorders [6-8]. sEMG also plays a critical role in prosthetic control, enabling recognition of motor intent and facilitating the operation of prosthetic limbs, exoskeletons, and assistive devices [9-11]. Moreover, sEMG finds applications in human-computer interaction systems, such as virtual reality, sign language recognition, and gaming, demonstrating its versatility [12-14].

However, acquiring and analyzing sEMG signals presents several challenges in both hardware and signal processing. Signals must pass through multiple tissue layers (fat, skin, and electrodes), resulting in low amplitudes (tens to hundreds of microvolts) that are highly susceptible to noise [15]. Common noise sources include powerline interference (50/60 Hz), motion artifacts from electrode displacement, crosstalk from adjacent muscles, and electronic noise from amplifiers. Additionally, inter- and intra-subject variability introduces further challenges for control [16]. Factors such as electrode placement, inter-electrode distance, orientation, proximity to innervation zones, skin properties, subcutaneous fat thickness, muscle fatigue, and posture changes can significantly affect signal amplitude and frequency content. Even slight shifts in electrode position can alter both time- and frequency-domain characteristics, reducing reproducibility and reliability in real-world applications. For embedded systems or assistive robotics, robustness to environmental variability and minimal recalibration requirements are essential.

Although sEMG-based HMI systems have been widely studied, most low-cost sEMG devices remain unsuitable for detailed finger-gesture analysis and real-time embedded use. Common limitations include a limited channel count, which restricts the observation of distributed forearm muscle activity [17, 18], restricted bandwidth or fixed analog front-end designs, which reduce sensitivity to low-amplitude muscle activations [15, 19], and a lack of access to raw sEMG data, as many systems provide only envelope-based or proprietary outputs [20]. Moreover, real-time embedded processing pipelines are often absent, with most implementations relying on PC-based computation, leading to increased latency and reduced portability [21]. These constraints significantly reduce their suitability for compact and wearable HMI applications that require low latency and access to raw sEMG signals. This work presents a compact and low-cost three-channel sEMG sensor co-designed with a lightweight real-time feature extraction pipeline, specifically targeting embedded gesture recognition under practical hardware constraints.

This study focuses on the design and development of a custom sEMG sensor along with appropriate signal processing methods for HMI. The objectives include: (i) building a low-cost, compact sEMG hardware suitable for human–machine applications (e.g., upper-limb exoskeletons or assistive devices), (ii) investigating preprocessing, feature extraction, and classification or regression algorithms to translate sEMG signals into control commands, and (iii) evaluating the performance of the proposed processing methods in terms of accuracy, latency, stability, and scalability across multiple users.

II. MATERIAL AND METHODS

A. *Custom sEMG Sensors*

This study outlines the physiological characteristics of sEMG signals and the resulting design requirements, followed by a detailed description of the proposed analog front-end and reference biasing scheme. Then, a comparison with existing sEMG systems is provided to position the proposed design within the current landscape.

sEMG signals are inherently weak bioelectrical signals. In healthy individuals, sEMG amplitudes typically range from 100 to 5000 µV, with peak values rarely exceeding 6000 µV, often close to the noise threshold. During muscle relaxation, sEMG amplitudes can be as low as 20–30 µV, whereas muscle contraction can increase amplitudes to 60–300 µV. In hemiplegic patients, these amplitudes tend to remain below 350 µV, making the signals more susceptible to external disturbances [12]. Frequency-domain analysis of sEMG signals indicates that the majority of the signal energy lies within 0–500 Hz, with the main energy concentrated between 20 and 150 Hz [19]. Based on these characteristics, a custom sEMG sensor is proposed, featuring a 2200× amplification and a bandwidth of 48–482 Hz. The sensor is designed to measure sEMG signals from the human forearm, and its detailed circuit schematic is illustrated in Figure 1.

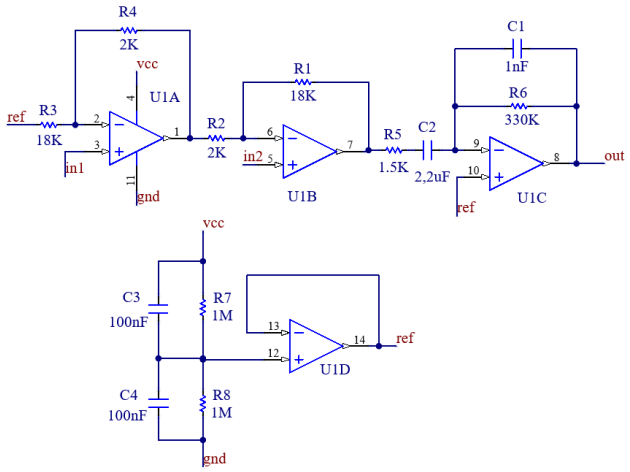

Fig. 1. Circuit schematic of the custom sEMG acquisition module showing differential amplifier stage (U1A, U1B), band-pass filter (U1C), and reference voltage generation (U1D).

The sensor employs dry electrodes and consists of three electrodes: "in1" and "in2" serve as the primary measurement electrodes, while "ref" functions as the reference electrode. The signal amplification stage is implemented using a differential amplifier followed by a band-pass filter. The objective is to safely amplify the microvolt-level differential signal to a level suitable for the ADC. The resulting output signal, denoted "out," is computed according to (1) and (2), under conditions $R_2 = R_4$ and $R_1 = R_3$.

$$V_{out} = A \times (V_{in1} - V_{in2}) + V_{ref} \quad (1)$$

$$A = A_1 \times A_2 = (1 + \frac{R_1}{R_4}) \times \frac{R_6}{R_5} = 2200 \quad (2)$$

The frequency filtering stage is implemented using a band-pass filter (U1C). sEMG signals with frequencies within the filter's passband are transmitted, while frequencies outside the passband are attenuated. The low and high cutoff frequencies are determined according to:

$$f_{c-high} = \frac{1}{2\pi R_6 C_2} = 482Hz \quad (3)$$

$$f_{c-low} = \frac{1}{2\pi R_5 C_1} = 48Hz \quad (4)$$

The reference electrode (ref) is biased at 2.5 V from a 5 V supply (Vcc) using a voltage divider and a buffer circuit (U1D). Since the microcontroller's ADC can only process positive analog signals, it cannot directly handle EMG signals with negative amplitudes. The reference voltage stage shifts the EMG signal baseline from 0 to 2.5 V, allowing the ADC to capture the full signal information. Figure 3 illustrates the resulting output of the sEMG sensor.

Several commercial and open-source sEMG acquisition systems, such as the Myo Armband, Ottobock 13E200, Delsys Trigno, and OpenBCI, have been widely employed in HMI research and rehabilitation applications. Commercial devices generally provide high signal quality and stable wireless transmission; however, high-end systems such as the Delsys Trigno are costly and rely on proprietary data formats, which restrict customization and low-level signal access [17]. More affordable solutions, especially the Myo Armband, offer only eight fixed channels with a limited bandwidth (5 to 200 Hz) [20], making it difficult to capture deeper or low-amplitude muscle activity. Meanwhile, open-source platforms such as OpenBCI provide greater flexibility but typically require bulky hardware components and are not optimized for real-time embedded control tasks [21]. Low-cost single-channel sEMG modules, such as MyoWare, are also widely used in educational and prototyping contexts [18]. The MyoWare sensor is limited to a single non-differential channel and relies on gel-based electrodes, which increases setup time and reduces long-term stability for wearable applications. Moreover, MyoWare outputs an analog envelope (rectified and smoothed) instead of raw sEMG data, preventing access to temporal signal fluctuations that are essential for feature extraction and classification. To better contextualize the proposed design, Table I presents a comparison with representative commercial and open-source sEMG acquisition systems.

TABLE I. COMPARISON OF THE PROPOSED SENSOR WITH EXISTING SEMG SYSTEMS

Criteria	Proposed module	MyoWare	OpenBCI	Myo Armband	Delsys Trigno
Channels	8	1	4-8	8	4-16
Bandwidth	48-482 Hz	~20–400 Hz	Configurable	5-200 Hz	20–450 Hz
Raw signal access	Yes (full raw data)	No (envelope only)	Yes	No (proprietary)	Yes (high fidelity)
Electrode type	Dry	Gel-based	Dry/gel	Dry	Dry
Approx. cost	Very Low	Low	medium	medium	Very High

Specifications are summarized from manufacturers' datasheets and published literature [20–23]

In comparison, the proposed custom sEMG module provides several advantages tailored for real-time human–machine interaction: (i) low-cost design using off-the-shelf analog front-end components; (ii) higher acquisition bandwidth (48–482 Hz) compared to many low-cost systems, improving sensitivity to rapid muscle activation dynamics; and (iii) compact integration with microcontrollers, enabling seamless embedding into wearable robotic or prosthetic devices without external amplifiers or communication modules. Although commercial systems remain valuable for laboratory-grade diagnostics, the proposed design provides a lightweight, low-latency, and customizable alternative optimized for real-time gesture recognition and embedded robotic control.

B. sEMG Signal Acquisition

Experiments were performed with one healthy male participant (age 25, no neuromuscular disorders). Ethical approval was granted under an internal institutional protocol, and informed consent was obtained before data collection. Dry electrodes were attached using an elastic armband to maintain stable skin contact and reduce motion artifacts during dynamic gestures. The skin surface was wiped with alcohol before placement to reduce impedance. The inter-electrode distance was set at 20 mm, and the reference electrode was fixed near the wrist region. The placement strictly followed anatomical landmarks as shown in Figure 2(b). This placement strategy selectively captures the muscle activities corresponding to specific finger movements, while maintaining a compact and reproducible configuration suitable for wearable applications.

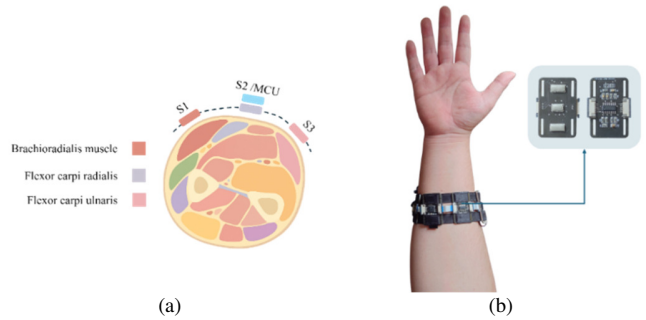

(a) (b)

Fig. 2. Electrode placement and experimental setup: (A) Cross-sectional schematic of the forearm showing sensor position (S1-S3) relative to the main muscle groups, (B) The custom sEMG sensor worn on the forearm with three acquisition channels connected to the processing unit.

The first sensor (S1) was positioned over the brachioradialis region, which is primarily associated with forearm flexion and the activation of the thumb during grasping and extension movements. The second sensor (S2) was located above the flexor carpi radialis, a muscle predominantly involved in the flexion of the wrist and activation of the index and middle fingers. This placement allows S2 to capture signals that contribute significantly to fine finger control and precision grips. The third sensor (S3) was placed near the flexor carpi ulnaris, which is responsible for wrist adduction and primarily contributes to the movement of the ring and little fingers.

This electrode configuration enables distributed measurement of muscle activity across the forearm, providing representative sEMG signals from both the radial and the ulnar sides. The spatial arrangement was optimized to reduce signal cross-talk between adjacent muscle groups while maintaining a compact form factor suitable for real-time HMI applications. Moreover, the selected muscle sites closely correspond to the major functional groups involved in grasping and finger flexion-extension, which are essential for future gesture classification and robotic control tasks.

The MCU acquires the sEMG signals and transmits the data via an RF24 wireless module. The device is powered by a lithium battery with an independent power management circuit to minimize electromagnetic interference from other sources. The acquisition frequency is set to 1000 Hz, in accordance with the Nyquist–Shannon sampling theorem, which requires a sampling rate greater than twice the signal bandwidth (representing the maximum frequency of the signal) [22]. For the sEMG sensor, the useful signal spectrum lies below 482 Hz. Moreover, the acquisition architecture is designed to be scalable, allowing future expansion to up to eight sEMG channels without significant modifications to the hardware.

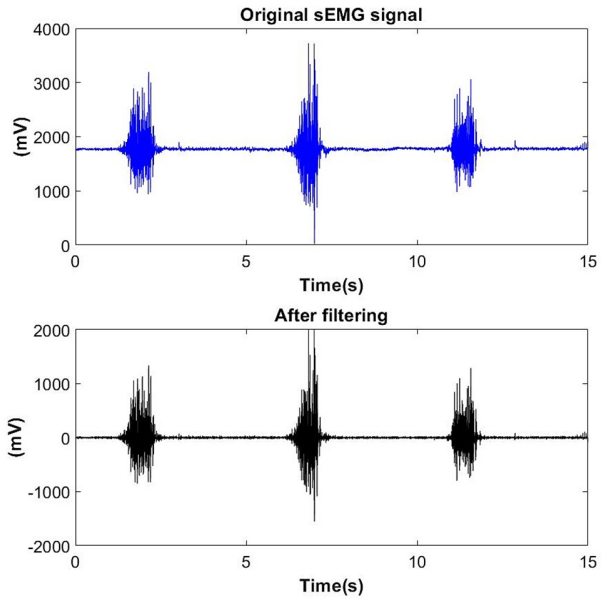

Fig. 3. Comparison between raw sEMG signal and processed signal after band-pass filtering (20–500 Hz) and 50 Hz notch filtering.

C. Digital Signal Processing

Various methods have been employed for processing sEMG signals. In general, the processing pipeline typically involves three main steps: filtering, segmentation, and feature extraction.

1) Filtering

Filtering is essential to minimize noise in sEMG signals. The most relevant information in sEMG is distributed within the 0 to 500 Hz frequency range, with the majority of the signal energy concentrated between 20 Hz and 150 Hz. Based on this characteristic, most studies employ band-pass filters with a typical frequency range of 20 to 500 Hz. The Butterworth band-pass filter is the most commonly used, with variations among studies primarily in filter order [7]. In [23], the necessity of applying a high-pass filter to remove low-frequency noise in sEMG signals was highlighted, recommending a cutoff frequency of around 20 Hz for natural movements, while high-intensity muscle activities may require a higher cutoff. In addition, a low-pass filter with a cutoff frequency between 400 and 500 Hz is often used to eliminate high-frequency noise. Notch filters can be applied to remove power-line interference from sEMG signals [24]; however, some researchers argue that such frequencies fall within the active range of sEMG and therefore omit notch filtering [25].

In this study, the sEMG signals were processed through a two-stage filtering procedure. First, a digital band-pass filter with a 20–500 Hz bandwidth was applied to remove low-frequency noise and eliminate the DC offset (2.5 V). The band-pass filter was implemented as a second-order Butterworth filter to ensure a flat frequency response within the passband and minimal signal distortion. Subsequently, a notch filter centered at 50 Hz was applied to suppress power-line interference.

To assess the signal quality of the proposed low-cost sEMG hardware, SNR was estimated using the standard definition:

$$SNR = 10\,log_{10}\left(\frac{P_{signal}}{P_{noise}}\right)\ (\text{dB}) \qquad (5)$$

where P_{signal} represents the average power of the sEMG signal during muscle activation, and P_{noise} is calculated from baseline measurements during muscle relaxation.

Across three channels (S1-S3) and multiple gesture trials, the computed SNR ranged between 17.8 and 22.5 dB, which is comparable to existing low-cost wearable sEMG systems [26], indicating that the analog front-end and bandwidth selection (48–482 Hz) effectively suppressed motion artifacts and electronic noise while preserving motor unit activation. The SNR achieved was sufficient to support the reliable extraction of amplitude-dependent features such as RMS, MAV, and WL, which further explains their robustness to noise and their strong discriminative ability across gestures.

2) Overlapped Sliding Window Segmentation

There are two common approaches for segmenting sEMG signals: the non-overlapping window method and the overlapping window method. In the non-overlapping window approach, the data are divided into predefined segments without overlap, and features are extracted from each segment. However, this technique has the drawback of requiring the processor to remain idle until the next segment is formed. In contrast, the overlapping window method involves segments that partially overlap with preceding segments, facilitating the extraction of additional features and often resulting in higher classification accuracy [27, 28].

In principle, this technique employs a sliding window with length w and step size s, where $s < w$, resulting in an overlap ratio $O = 1 - s/w$. The window length (w) determines the amount of EMG data used for feature extraction, while the step size (s) controls the temporal spacing between windows and governs the sliding rate. This approach ensures that consecutively extracted features maintain temporal continuity, enabling classification or motion recognition models to track signal variations more smoothly.

The choice of window length w and step size s is critical, directly affecting feature stability, system latency, and overall classification performance. The window length specifies the number of signal samples used to compute features. Increasing w incorporates more samples per window, reducing the variance of feature estimates and enhancing the stability of time-domain features such as Mean Absolute Value (MAV), Root Mean Square (RMS), and Variance (VAR). However, excessively long windows can decrease temporal resolution, causing the system to respond more slowly to rapid muscle activity changes. The step size determines the interval between successive windows, which corresponds to the feature update rate and decision frequency. With an overlap ratio O, decreasing s (i.e., increasing overlap) allows more frequent updates, improves temporal continuity of features, and reduces fluctuations between windows. Conversely, very small step sizes can increase computational load, particularly in embedded systems.

Several studies have investigated optimal window sizes for sEMG signals [29, 30], suggesting an optimal window range of 100–250 ms. In [31], SVM classifiers achieved the best performance with a window length of 240 ms and a step size of 120 ms (50% overlap). In this study, the window length (w) was set to 200 ms and the step size (s) to 100 ms, as illustrated in Figure 4. With a sampling frequency of 1 kHz, each window corresponds to 200 samples. As the window slides by 100 samples, a 50% overlap occurs between consecutive windows.

3) Feature Extraction

Feature extraction not only enhances classifier performance but also reduces data dimensionality, simplifying subsequent processing and classification [30]. Features can generally be categorized into three types: time-domain, frequency-domain, and time–frequency domain features. Time-domain feature extraction is widely used and efficient for characterizing sEMG signals, offering low computational complexity, which makes it particularly suitable for real-time control systems. Time-domain features are particularly advantageous for real-time embedded applications because they require only basic arithmetic operations and do not rely on signal transformations such as FFT or wavelet decomposition. Their computation can be executed within a few milliseconds on low-power

microcontrollers, making them suitable for continuous gesture tracking and low-latency control. Additionally, these features can be extracted on sliding windows with minimal memory usage, allowing high update rates. Table II provides a summary of commonly used time-domain features.

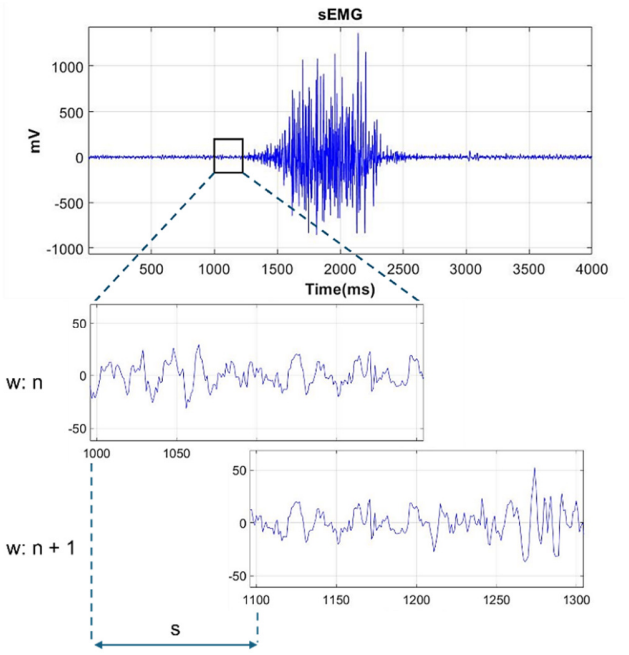

Fig. 4. Overlapping sliding window segmentation with 200 ms window length and 100 ms step size (50% overlap).

TABLE II. SUMMARY OF TIME-DOMAIN FEATURES

Feature	Formula	Explanation
Mean Absolute Value (MAV)	$MAV = \frac{1}{N}\sum_{i=1}^{N}\lvert x_i\rvert$	Average of absolute values; indicates muscle activation level.
Waveform Length (WL)	$WL = \sum_{i=1}^{N-1}\lvert x_{i+1} - x_i\rvert$	Sum of absolute change; measures signal complexity.
Zero Crossing (ZC)	$ZC = \sum_{i=1}^{N-1}\begin{bmatrix}\text{sgn}(x_i \times x_{i+1}) \\ \cap\lvert x_i - x_{i+1}\rvert \geq threshold\end{bmatrix}$	Counts sign changes; relates to frequency content
Variance (VAR)	$VAR = \frac{1}{N-1}\sum_{i=1}^{N} x_i^2$	Energy dispersion around mean; reflects contraction intensity.
Root Mean Square (RMS)	$RMS = \sqrt{\frac{1}{N}\sum_{i=1}^{N} x_i^2}$	Effective signal power; correlates with muscle force.
Slope sign change (SSC)	$SSC = \sum^{N-1}\begin{bmatrix}f[(x_i - x_{i-1}) \\ \times(x_i - x_{i-1})]\end{bmatrix}$	Counts slope direction changes; indicates signal fluctuation.
Integrate EMG (IEMG)	$IEMG = \sum_{i=1}^{N}\lvert x_i\rvert$	Cumulative muscle activity over time.

x_i denotes the i^{th} sample of the sEMG signal within a segment of N samples.
$f[.]$ is a binary function returning 1 if the condition is true, otherwise 0.

In contrast to time-domain features, frequency-domain features cannot be directly obtained from raw data and require the application of a Fourier transform to the signal. The Power Spectral Density (PSD) of an sEMG signal represents the distribution of signal energy across different frequency components [32]. PSD is typically estimated using Fourier-based methods (e.g., the Welch method) from finite-time signal data. From the PSD, two primary frequency-domain features can be derived: Mean Frequency (MNF) and Median Frequency (MDF). MNF is calculated as the power-weighted average of frequencies, while MDF is the frequency that divides the spectrum into two halves, each containing half of the total power. For a symmetric spectrum, MNF and MDF coincide; however, sEMG spectra are typically skewed toward lower frequencies, resulting in MDF values generally smaller than MNF [33-36]. Time-Frequency Domain (TFD) features combine temporal and spectral information, enabling observation of different frequency components at different time intervals. TFD analysis is particularly valuable for capturing localized, transient, or non-stationary components that are often overlooked by purely spectral methods such as FFT [37]. Various approaches, including Continuous Wavelet Transform (CWT) and Discrete Wavelet Transform (DWT), are available for analyzing signals in the time-frequency plane, each offering distinct advantages depending on the application.

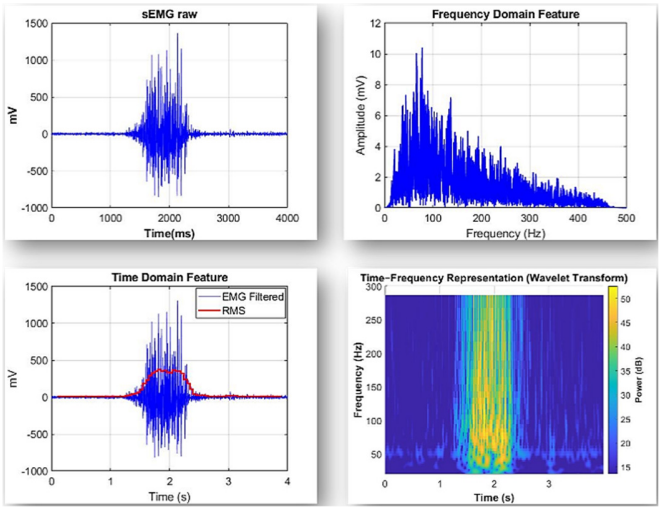

Fig. 5. Analysis of sEMG signals: raw sEMG signal, extracted time-domain features, frequency-domain representation (PSD), and time-frequency representation using wavelet transform.

III. RESULTS AND DISCUSSIONS

The custom sEMG sensor was evaluated using three channels (S1–S3) during three hand gestures: gesture 2 (index finger movement), the OK sign, and hand grasp (Figure 6). The three-channel configuration reliably captured distinct muscle activation patterns corresponding to each gesture, demonstrating sensitivity to both subtle and strong contractions. Time-domain features, Root Mean Square (RMS), Waveform Length (WL), and Variance (VAR), proved to be the most robust and discriminative across gestures.

RMS values increased proportionally with the level of contraction, showing the highest amplitudes during hand grasp, moderate levels for the OK sign, and the lowest values for

isolated index finger movement. WL and VAR further reflected the complexity and variability of muscle activation, providing clear separation among gestures. Due to the high-gain amplification stage (2200×) and optimized 48–482 Hz bandwidth, these amplitude-based features remained resilient to baseline fluctuations and motion artifacts, even under weak contractions.

To further assess the robustness of the proposed hardware and feature extraction pipeline, a repeatability test was conducted using the same subject performing each gesture across five repeated trials. Time-domain features (RMS, WL, VAR) were extracted from the three channels using the same sliding window configuration. The results showed that RMS and WL maintained low variability (<5%) across trials, while VAR exhibited slightly higher variations (≈7-10%) during weak contractions but remained consistent in trend across gestures. These findings confirm that the custom low-cost hardware can generate reproducible features suitable for embedded real-time classification. Across repeated trials, RMS, WL, and VAR demonstrated high consistency and reproducibility, while baseline drift and noise remained minimal. In contrast, features such as Zero Crossing (ZC) and Slope Sign Change (SSC) exhibited greater sensitivity to minor noise fluctuations and electrode positioning, making them less suitable for low-cost, shallow-depth sEMG hardware.

These findings indicate that the selected time-domain features align well with both the hardware configuration and the signal quality achievable from the low-cost 3-channel acquisition module. Therefore, RMS, WL, and VAR are recommended as primary inputs for real-time embedded classification algorithms. Overall, the results confirm that the proposed sensor can effectively capture forearm muscle activity and extract highly reliable features for practical implementation in wearable systems such as robotic exoskeletons, prosthetics, etc.

Although no external latency benchmark was recorded, the computational delay can be estimated from the sliding window configuration. With a window length of 200 ms and 50% overlap, a new feature vector is produced every 100 ms, resulting in an effective latency below 0.1 s. This level of delay is widely considered acceptable for real-time sEMG-controlled HMI applications and has been reported in comparable studies.

Although the proposed sensor demonstrates stable performance during controlled experiments, several limitations should be acknowledged. First, the current hardware employs a fixed amplification gain (2200×), which may not be optimal for different muscle groups or users with weak muscle activation. Second, minor electrode displacement and motion artifacts can still influence the extracted features during prolonged wearable use. Third, inter-subject variability was not assessed, as this study focused on validating the hardware with a single participant. Future work will incorporate adjustable gain control and cross-user evaluation to enhance the versatility and robustness of the system in practical environments.

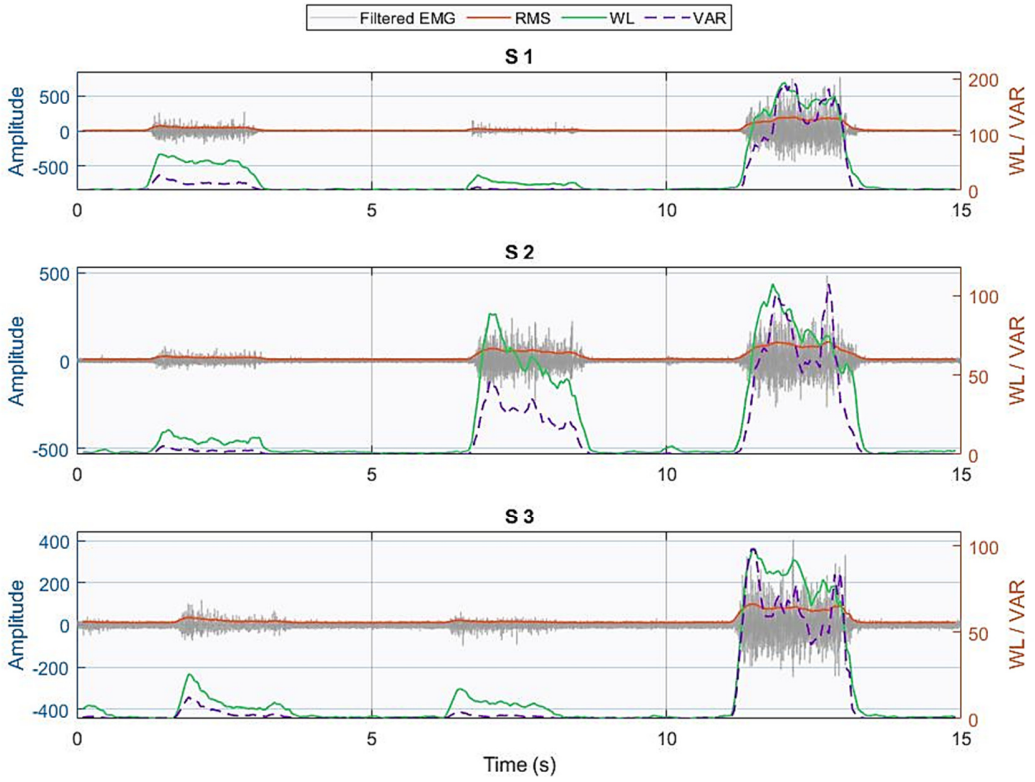

Fig. 6. Time-domain features (RMS, WL, VAR) extracted from three sEMG channels (S1–S3) during three hand gestures: gesture 2, OK sign, and hand grasp.

IV. CONCLUSIONS AND FUTURE WORK

This study presented a custom sEMG sensor and associated feature extraction methods for HMI applications. The proposed sensor was designed to offer both functional performance and practical usability. Compared with existing systems, it is low-cost, compact, and wearable, making it suitable for long-term or mobile usage. The use of dry electrodes eliminates the need for conductive gel and allows quick placement on forearm muscles, while still maintaining stable contact and reducing cross-talk between adjacent muscle groups. sEMG signals were collected from three channels during multiple hand gestures, and features were extracted from different domains, including the time domain (RMS, WL, VAR), frequency domain, and time-frequency domain, providing a comprehensive representation of muscle activity. The results show that the sensor reliably captures distinct activation patterns and time-domain features in particular, demonstrating clear discriminatory power between gestures. These findings confirm that the custom sensor is sensitive, stable, and capable of generating high-quality features suitable for real-time gesture recognition and control tasks.

The experimental results confirmed that the proposed hardware achieves adequate signal quality and stability for real-time embedded applications. Across three forearm channels, the measured SNR ranged from 17.8 to 22.5 dB, while repeatability tests over five trials showed low variability for amplitude-based features (<5% for RMS and WL, 7–10% for VAR during weak contractions). With a 200 ms sliding window and 50% overlap, the effective processing latency was estimated to be below 0.1 s, satisfying real-time HMI requirements. These results demonstrate that the proposed sEMG module can reliably capture forearm muscle activity and extract stable, discriminative time-domain features (RMS, WL, VAR) that are well suited to low-cost, resource-constrained embedded systems, offering a practical alternative to more complex or proprietary sEMG platforms.

Future work will focus on extending the current system towards real-time gesture recognition. Specifically, the next research phase will investigate classification models based on machine learning and deep learning (e.g., SVM, CNN, LSTM, and Transformer-based architectures) using the extracted multi-domain features. In addition, feature selection strategies and cross-user evaluation will be conducted to assess robustness and improve generalization across different subjects. Ultimately, the system will be integrated into wearable HMI devices (robotic prosthetics and exoskeletons) to achieve responsive and user-adaptive control with low computational latency.

DATA AVAILABILITY

The data supporting the findings of this study were acquired under an internal ethics protocol and are therefore not publicly available. Limited access may be granted upon reasonable request for academic research purposes only.

ACKNOWLEDGMENT

This work presents the research findings of Project No. ĐTKHCN.05/2025, an institutional-level research project at Electric Power University in 2025.

REFERENCES

[1] E. A. Clancy, E. L. Morin, G. Hajian, and R. Merletti, "Tutorial. Surface electromyogram (sEMG) amplitude estimation: Best practices," *Journal of Electromyography and Kinesiology*, vol. 72, Oct. 2023, Art. no. 102807, https://doi.org/10.1016/j.jelekin.2023.102807.

[2] N. K. Nguyen, T. M. P. Dao, T. D. Nguyen, D. T. Nguyen, H. T. Nguyen, and V. K. Nguyen, "An sEMG Signal-based Robotic Arm for Rehabilitation applying Fuzzy Logic," *Engineering, Technology & Applied Science Research*, vol. 14, no. 3, pp. 14287–14294, June 2024, https://doi.org/10.48084/etasr.7146.

[3] Q. Ai, Y. Zhang, W. Qi, Q. Liu, and A. K. Chen, "Research on Lower Limb Motion Recognition Based on Fusion of sEMG and Accelerometer Signals," *Symmetry*, vol. 9, no. 8, Aug. 2017, Art. no. 147, https://doi.org/10.3390/sym9080147.

[4] X. Wang, C. Zhang, Z. Yu, and C. Deng, "Decoding of lower limb continuous movement intention from multi-channel sEMG and design of adaptive exoskeleton controller," *Biomedical Signal Processing and Control*, vol. 94, Aug. 2024, Art. no. 106245, https://doi.org/10.1016/j.bspc.2024.106245.

[5] D. Borzelli, S. Pastorelli, and L. Gastaldi, "Determination of the Human Arm Stiffness Efficiency with a Two Antagonist Muscles Model," in *Advances in Italian Mechanism Science*, vol. 47, G. Boschetti and A. Gasparetto, Eds. Springer International Publishing, 2017, pp. 71–78.

[6] H. Hellara, R. Barioul, S. Sahnoun, A. Fakhfakh, and O. Kanoun, "Comparative Study of sEMG Feature Evaluation Methods Based on the Hand Gesture Classification Performance," *Sensors*, vol. 24, no. 11, June 2024, Art. no. 3638, https://doi.org/10.3390/s24113638.

[7] A. Leone, A. M. Carluccio, A. Caroppo, A. Manni, and G. Rescio, "A Systematic Review of Surface Electromyography in Sarcopenia: Muscles Involved, Signal Processing Techniques, Significant Features, and Artificial Intelligence Approaches," *Sensors*, vol. 25, no. 7, Mar. 2025, Art. no. 2122, https://doi.org/10.3390/s25072122.

[8] M. Al-Ayyad, H. A. Owida, R. De Fazio, B. Al-Naami, and P. Visconti, "Electromyography Monitoring Systems in Rehabilitation: A Review of Clinical Applications, Wearable Devices and Signal Acquisition Methodologies," *Electronics*, vol. 12, no. 7, Mar. 2023, Art. no. 1520, https://doi.org/10.3390/electronics12071520.

[9] D. Zhao *et al.*, "Upper limb human-exoskeleton system motion state classification based on semg: application of CNN-BiLSTM-attention model," *Scientific Reports*, vol. 15, no. 1, May 2025, Art. no. 18969, https://doi.org/10.1038/s41598-025-02864-5.

[10] X. Zhang, Y. Qu, G. Zhang, Z. Wang, C. Chen, and X. Xu, "Review of sEMG for Exoskeleton Robots: Motion Intention Recognition Techniques and Applications," *Sensors*, vol. 25, no. 8, Apr. 2025, Art. no. 2448, https://doi.org/10.3390/s25082448.

[11] Z. Mhiriz, M. Bourhaleb, and M. Rahmoune, "Leveraging Machine Learning for Signal Processing in Surface Electromyography (sEMG) for Prosthetic Control," in *Digital Technologies and Applications*, vol. 1098, S. Motahhir and B. Bossoufi, Eds. Springer Nature Switzerland, 2024, pp. 107–116.

[12] J. Wu, X. Li, W. Liu, and Z. Jane Wang, "sEMG Signal Processing Methods: A Review," *Journal of Physics: Conference Series*, vol. 1237, no. 3, June 2019, Art. no. 032008, https://doi.org/10.1088/1742-6596/1237/3/032008.

[13] Y. Liu, X. Li, L. Yang, and H. Yu, "A Transformer-Based Gesture Prediction Model via sEMG Sensor for Human–Robot Interaction," *IEEE Transactions on Instrumentation and Measurement*, vol. 73, pp. 1–15, 2024, https://doi.org/10.1109/TIM.2024.3373045.

[14] J. W. Liang, H. W. Feng, B. Zhang, J. M. Liang, Y. W. Liu, and Z. H. Li, "A Convolutional Neural Network Classification Method Based on Non-Ideal sEMG Signals for Human-Robot Interaction System," in *2025 37th Chinese Control and Decision Conference (CCDC)*, Xiamen,

China, May 2025, pp. 2474–2479, https://doi.org/10.1109/CCDC65474.2025.11090507.

[15] I. Karacan and K. S. Türker, "A comparison of electromyography techniques: surface versus intramuscular recording," *European Journal of Applied Physiology*, vol. 125, no. 1, pp. 7–23, Jan. 2025, https://doi.org/10.1007/s00421-024-05640-x.

[16] T. Song, Z. Yan, S. Guo, Y. Li, X. Li, and F. Xi, "Review of sEMG for Robot Control: Techniques and Applications," *Applied Sciences*, vol. 13, no. 17, Aug. 2023, Art. no. 9546, https://doi.org/10.3390/app13179546.

[17] K. Challa, I. W. AlHmoud, C. Jaiswal, A. C. Turlapaty, and B. Gokaraju, "EMG features dataset for arm activity recognition," *Data in Brief*, vol. 60, June 2025, Art. no. 111519, https://doi.org/10.1016/j.dib.2025.111519.

[18] M. O. Arregi and E. L. Secco, "A Low-Cost EMG Graphical User Interface Controller for Robotic Hand," in *Proceedings of the Future Technologies Conference (FTC) 2021, Volume 2*, vol. 359, K. Arai, Ed. Springer International Publishing, 2022, pp. 459–475.

[19] T. W. Beck, J. M. DeFreitas, and M. S. Stock, "The Effects of a Resistance Training Program on Average Motor Unit Firing Rates.," *Clinical Kinesiology (Online Edition)*, 2011.

[20] I. Mendez *et al.*, "Evaluation of the Myo armband for the classification of hand motions," in *2017 International Conference on Rehabilitation Robotics (ICORR)*, London, UK, July 2017, pp. 1211–1214, https://doi.org/10.1109/ICORR.2017.8009414.

[21] T. Mahboob, M. Y. Chung, and K. W. Choi, "EMG-based 3D hand gesture prediction using transformer–encoder classification," *ICT Express*, vol. 9, no. 6, pp. 1047–1052, Dec. 2023, https://doi.org/10.1016/j.icte.2023.04.005.

[22] B. Chen *et al.*, "A Real-Time EMG-Based Fixed-Bandwidth Frequency-Domain Embedded System for Robotic Hand," *Frontiers in Neurorobotics*, vol. 16, June 2022, Art. no. 880073, https://doi.org/10.3389/fnbot.2022.880073.

[23] C. J. De Luca, L. Donald Gilmore, M. Kuznetsov, and S. H. Roy, "Filtering the surface EMG signal: Movement artifact and baseline noise contamination," *Journal of Biomechanics*, vol. 43, no. 8, pp. 1573–1579, May 2010, https://doi.org/10.1016/j.jbiomech.2010.01.027.

[24] J. C. Kline and C. J. De Luca, "Error reduction in EMG signal decomposition," *Journal of Neurophysiology*, vol. 112, no. 11, pp. 2718–2728, Dec. 2014, https://doi.org/10.1152/jn.00724.2013.

[25] C. Li, H. He, S. Yin, H. Deng, and Y. Zhu, "Continuous Angle Prediction of Lower Limb Knee Joint Based on sEMG," in *2021 IEEE International Conference on Recent Advances in Systems Science and Engineering (RASSE)*, Shanghai, China, Dec. 2021, pp. 1–6, https://doi.org/10.1109/RASSE53195.2021.9686816.

[26] A. Bawa and K. Banitsas, "Design Validation of a Low-Cost EMG Sensor Compared to a Commercial-Based System for Measuring Muscle Activity and Fatigue," *Sensors*, vol. 22, no. 15, Aug. 2022, Art. no. 5799, https://doi.org/10.3390/s22155799.

[27] N. Nazmi, M. Abdul Rahman, S. I. Yamamoto, S. Ahmad, H. Zamzuri, and S. Mazlan, "A Review of Classification Techniques of EMG Signals during Isotonic and Isometric Contractions," *Sensors*, vol. 16, no. 8, Aug. 2016, Art. no. 1304, https://doi.org/10.3390/s16081304.

[28] T. R. Farrell and R. F. Weir, "The Optimal Controller Delay for Myoelectric Prostheses," *IEEE Transactions on Neural Systems and Rehabilitation Engineering*, vol. 15, no. 1, pp. 111–118, Mar. 2007, https://doi.org/10.1109/TNSRE.2007.891391.

[29] H. Ashraf *et al.*, "Evaluation of windowing techniques for intramuscular EMG-based diagnostic, rehabilitative and assistive devices," *Journal of Neural Engineering*, vol. 18, no. 1, Feb. 2021, Art. no. 016017, https://doi.org/10.1088/1741-2552/abcc7f.

[30] F. Kulwa, O. W. Samuel, M. G. Asogbon, O. O. Obe, and G. Li, "Analyzing the Impact of Varied Window Hyper-parameters on Deep CNN for sEMG based Motion Intent Classification," in *2022 IEEE International Workshop on Metrology for Industry 4.0 & IoT (MetroInd4.0&IoT)*, Trento, Italy, June 2022, pp. 81–86, https://doi.org/10.1109/MetroInd4.0IoT54413.2022.9831573.

[31] L. H. Smith, L. J. Hargrove, B. A. Lock, and T. A. Kuiken, "Determining the Optimal Window Length for Pattern Recognition-Based Myoelectric Control: Balancing the Competing Effects of Classification Error and Controller Delay," *IEEE Transactions on Neural Systems and Rehabilitation Engineering*, vol. 19, no. 2, pp. 186–192, Apr. 2011, https://doi.org/10.1109/TNSRE.2010.2100828.

[32] H. F. Hassan, S. J. Abou-Loukh, and I. K. Ibraheem, "Teleoperated robotic arm movement using electromyography signal with wearable Myo armband," *Journal of King Saud University - Engineering Sciences*, vol. 32, no. 6, pp. 378–387, Sept. 2020, https://doi.org/10.1016/j.jksues.2019.05.001.

[33] S. Said, Z. Albarakeh, T. Beyrouthy, S. Alkork, and A. Nait-ali, "Machine-Learning based Wearable Multi-Channel sEMG Biometrics Modality for User's Identification," in *2021 4th International Conference on Bio-Engineering for Smart Technologies (BioSMART)*, Paris/Créteil, France, Dec. 2021, pp. 1–4, https://doi.org/10.1109/BioSMART54244.2021.9677744.

[34] T. Stefanou, D. Guiraud, C. Fattal, C. Azevedo-Coste, and L. Fonseca, "Frequency-Domain sEMG Classification Using a Single Sensor," *Sensors*, vol. 22, no. 5, Mar. 2022, Art. no. 1939, https://doi.org/10.3390/s22051939.

[35] C. K. Chan, G. F. Timothy, and C. H. Yeow, "Comparison of mean frequency and median frequency in evaluating muscle fiber type selection in varying gait speed across healthy young adult individuals," in *2016 38th Annual International Conference of the IEEE Engineering in Medicine and Biology Society (EMBC)*, Orlando, FL, USA, Aug. 2016, pp. 1725–1728, https://doi.org/10.1109/EMBC.2016.7591049.

[36] B. N. Cahyadi *et al.*, "Analysis of EMG based Arm Movement Sequence using Mean and Median Frequency," in *2018 5th International Conference on Electrical Engineering, Computer Science and Informatics (EECSI)*, Malang, Indonesia, Oct. 2018, pp. 440–444, https://doi.org/10.1109/EECSI.2018.8752777.

[37] A. Phinyomark, P. Phukpattaranont, and C. Limsakul, "Feature reduction and selection for EMG signal classification," *Expert Systems with Applications*, vol. 39, no. 8, pp. 7420–7431, June 2012, https://doi.org/10.1016/j.eswa.2012.01.102.